THEORETICAL FRAMEWORK FOR PREDICTING THE RESPONSE OF TOLERABLY MOBILE SUBSEA INSTALLATIONS

Published in Géotechnique 67(7):608-620 http://dx.doi.org/10.1680/jgeot.16.P.137

Michael L. COCJIN (BEng, MEng) (corresponding author)

Centre for Offshore Foundation Systems – M053,

A node of ARC Centre for Geotechnical Science and Engineering

University of Western Australia

35 Stirling Highway, Crawley, Perth, WA 6009, Australia

Tel: +61 8 6488 3995, Fax: +61 8 6488 1044

Email: michael.cocjin@research.uwa.edu.au

Susan M. GOURVENEC (BEng, PhD)

Centre for Offshore Foundation Systems, UWA

A node of the ARC Centre for Geotechnical Science and Engineering

Email: susan.gourvenec@uwa.edu.au

David J. WHITE (MA, MEng, PhD)

Centre for Offshore Foundation Systems, UWA

A node of the ARC Centre for Geotechnical Science and Engineering

Email: david.white@uwa.edu.au

Mark F. RANDOLPH (MA, PhD, FAA, FREng, FRS, FTSE, FIEAust, CPEng)

Centre for Offshore Foundation Systems, UWA

A node of the ARC Centre for Geotechnical Science and Engineering

Email: mark.randolph@uwa.edu.au

No. of words: 5,507

No. of tables: 2

No. of figures: 15

Abstract:

Tolerable mobility of subsea foundations and pipelines supporting offshore oil and gas developments has recently become an accepted design concept. It enables a smaller foundation footprint and so is a potential cost-saving alternative to conventionally engineered ‘fixed’ seabed foundations. Dominant sources of loading on subsea infrastructure arise from connection misalignment or thermal and pressure induced expansion and these are reduced if the structure is permitted to displace while ensuring that additional loading is not induced by excessive settlements. A sound prediction of the resulting sliding response will provide a robust design basis for mobile subsea infrastructure. This paper presents a theoretical model based on critical state soil mechanics to predict the performance of a subsea installation that is founded on soft normally consolidated or lightly overconsolidated soil, and subjected to intermittent horizontal sliding movements. The framework is validated against centrifuge test results and is shown to capture the essential elements of the soil-structure interaction, which include (i) the changing soil strength from cycles of sliding and pore pressure generation, (ii) the regain in strength due to dissipation of excess pore pressure (consolidation), and (iii) the soil contraction and consequent settlement of the foundation caused by the consolidation process.

Key words: Foundation, consolidation, critical state soil mechanics

1. INTRODUCTION

Subsea facilities to support oil and gas developments include pipelines and associated structures that experience significant loads from thermal and pressure-induced expansions, as well as connector misalignment. These loads are relieved if the infrastructure can move, so the conventional design approach of aiming to eliminate plastic movements or to resist factored maximum loads can be inefficient. Instead, an emerging design philosophy is to allow foundations and pipelines to move back and forth in response to such loads, subject to other criteria such as ensuring that the associated settlements do not cause unacceptable secondary loads (Fisher & Cathie, 2003; Cocjin *et al.*, 2014; Deeks *et al.*, 2014).

For robust design of such tolerably mobile seabed infrastructure, it is necessary to predict the changing seabed resistance through cycles of infrastructure movement, and also the accumulating settlements. The framework presented in this paper provides these predictions by applying a methodology based on critical state soil mechanics that is appropriate for soft normally-consolidated or lightly-overconsolidated soil. The framework is validated against centrifuge test results of a tolerably mobile sliding subsea foundation but is equally applicable to other boundary value problems that involve horizontal shearing at the mudline, such as axial walking of seabed pipelines.

2. MOTIVATION

To predict the resistance and settlement of a seabed installation during episodes of horizontal movement and intervening periods of consolidation, three key elements are required: (i) the undrained strength associated with large strains that cause remoulding, and the associated pore pressure generation, (ii) the changes in strength due to dissipation of the excess pore pressure (consolidation), and (iii) the contraction and consequent settlement caused by the consolidation process.

Previous research on shallow foundations under cyclic loading has mainly focused on events that are fully undrained, such as for conditions beneath a typical gravity-based platform during a design storm event (e.g. Andersen, 1976; Andersen, 2009; Xiao et al. 2016). Some studies have investigated the subsequent change in soil strength due to reconsolidation (e.g. France & Sangrey, 1977), but the timescales are such that this has limited practical relevance for fixed surface-piercing offshore platforms founded on clay. Subsea infrastructure is supported on foundations of smaller dimension than for a gravity based or jacket platform and the governing load cases are typically caused by thermal expansion or operating pressures in pipelines, which have a much longer cyclic period – typically days or weeks – so significant consolidation can occur between load cycles.

The combined effects on soil strength and infrastructure settlement of cycles of loading and consolidation can be captured via an effective stress framework based on critical state concepts. Such a framework has been proposed previously to analyse the cyclic remoulding and reconsolidation processes during penetration of a cylinder into the seabed, such as a T-bar penetrometer or a pipeline element (White and Hodder, 2010; Hodder *et al.*, 2013). In this analysis, the degradation of soil strength comes from the gross remoulding of the soil around the pipe due to cyclic vertical movement.

In the case of an installation moving horizontally at the soil surface, the shearing process is concentrated close to the surface, as illustrated by analyses of a pipeline sliding over soft clay presented by Yan *et al.* (2014). In this case the associated generation of excess pore pressure varies with depth according to the distribution of mobilised shear stress. Through cycles of sliding and reconsolidation, the surrounding soil gains strength from episodes of undrained failure followed by pore pressure dissipation and contraction. In the present paper, this behaviour is idealised as one-dimensional – in an extension of the widely-used oedometer method for foundation settlement (Skempton & Bjerrum, 1957) – and both the settlement and the evolving sliding resistance are calculated on a cycle-by-cycle basis. This methodology provides a practical tool to support the design of tolerably mobile subsea installations.

3. OVERVIEW OF THE FRAMEWORK

The problem addressed in this study is illustrated in **Fig. 1**. An infinite half space is considered with a constant vertical stress applied at the mudline, σ_{op}, representing the submerged self-weight of the subsea facility. Cycles of horizontal shear stress, τ_{op}, in alternating directions are applied at the mudline to represent the effect of the sliding movement, δu, of the infrastructure. Sliding is assumed to take place at a rate that causes an undrained soil response, with intervening periods of consolidation between each shear stress reversal. The half-space is idealised as a one-dimensional column of soil elements, each subject to a vertical total stress and cycles of horizontal shear stress, and responding according to a simple form of critical state model. The framework can be applied in a cycle-by-cycle manner, solving for the response at each soil element to determine the cumulative change in void ratio and the variation in shear stress and settlement at the soil surface. Key elements of the framework include:

(i) Profiles of vertical stress and horizontal shear stress with depth, proportional to σ_{op} and τ_{op};

(ii) A critical state model for undrained shear strength, s_u, defined in the volumetric plane in terms of void ratio, e, and vertical effective stress, σ'_v, and in the stress plane in terms of s_u and σ'_v, which defines the current undrained strength and the excess pore pressure generated during shearing to failure. A critical state line (CSL) is defined in the usual way and is reached when the soil is first sheared to failure. However, the CSL is not fixed in the volumetric plane but instead migrates towards a limiting lower void ratio as a result of on-going cycles of shearing.

(iii) Simple scaling rules for cycles of shear stress that do not cause failure of the soil element, to determine the generated excess pore pressure in pre-failure cycles and the equivalent fraction of a full cycle of shearing, to determine the CSL migration.

The imposed soil stresses during shearing cycles on a soil element located at a depth, z below the surface, are the total vertical stress, σ_v and shear stress, τ. These are defined as proportions of the surface values by influence factors I_σ and I_τ that scale the distribution of vertical and shear stresses with depth ($I_\sigma = I_\tau = 1$ at $z = 0$ and $I_\sigma = I_\tau \rightarrow 0$ for $z \rightarrow \infty$) (with the geostatic vertical stress superimposed). Solutions for stress profiles with depth are presented by Poulos & Davis (1974) for different surface loading configurations on an elastic half space.

The critical state framework is defined in terms of the vertical stress and horizontal shear stress acting in the ground (**Fig. 1**), since these are more convenient inputs than the mean principal effective stress, p', and the deviatoric stress, q, for the boundary conditions being considered. This simplification is similar to the approach adopted by White & Hodder (2010) and Hodder *et al.* (2013) for cyclic penetrometer resistance.

Figure 2 illustrates a critical state interpretation of the problem, in terms of the state and stress paths in (**a**) $\sigma'_v - e$, and (**b**) $\sigma'_v - \tau$ planes, respectively.

An initially normally consolidated, (point A in **Fig. 2(a)**) or lightly over consolidated soil (point B) is considered. During undrained shearing, for instance from sliding of a surface foundation or pipeline, positive excess pore pressure is generated, $\Delta u_{e,gen} > 0$, resulting in a decrease of the effective vertical stress, σ'_v. The stress state moves towards the CSL at constant void ratio, e. Unless the soil profile has a weaker layer at depth, the soil element at the mudline level will fail, so the stress state reaches the CSL (B to C in **Fig. 2(a)**). Elements of soil at depth will move towards, but not reach the critical state line (B to C'), at least during the initial cycle. At the critical state, the current undrained shear strength is mobilised (C in **Fig. 2(b)**).

During the subsequent period of consolidation, the excess pore pressures dissipate ($\Delta u_{e,dis}$ through C – D in **Fig. 2**, or with partial consolidation terminating at D') and the effective vertical stress returns towards the initial condition, i.e. $\sigma_v = \sigma'_v$. The increase in σ'_v follows the unload-reload line (URL), defined by slope κ, causing a decrease in the void ratio (Δe), and an accumulation of settlement at the soil surface. The shear stress could be sustained during this period, or could decay (if the infrastructure is held at a fixed position, for example), but for simplicity the framework does not distinguish between these cases.

During subsequent shearing cycles the soil element will fail at a higher vertical effective stress, σ'_v (D – E, **Fig. 2(a)**) and consequentially mobilise a larger shear stress at failure (E in **Fig. 2(b)**).

4. COMPONENTS OF THE FRAMEWORK

Figure 3 presents the components of the framework in the order that they are required to perform a cycle-by-cycle calculation. The components are introduced in the same sequence below.

(a) *Vertical equilibrium conditions*

The framework first considers vertical equilibrium of the soil mass under the applied vertical stress at the surface and the soil self-weight stresses (**Fig. 3(a)**). The equilibrium vertical effective stress at depth z is:

$$\sigma'_{v,eqm} = \sigma'_{v0} + \sigma_{op} \cdot I_\sigma \tag{1}$$

where σ'_{v0} is the in situ soil self-weight vertical effective stress, equivalent to $\gamma'_{av} \cdot z$ with γ'_{av} being the average effective unit weight of the overlying soil, σ_{op} is the applied vertical stress at the surface, due to the submerged self-weight of the infrastructure, and I_σ is the influence factor defining the distribution of applied vertical stress with depth.

The void ratio at the state of equilibrium, e_{eqm}, is defined as:

$$e_{eqm} = \mathrm{N} - \lambda \ln\left(OCR \cdot \sigma'_{v,eqm}\right) + \kappa \ln\left(OCR\right) + \Delta e_i \left(\frac{\sigma'_{v,i}}{OCR \cdot \sigma'_{v,eqm}}\right)^{b_{NCL}} \tag{2}$$

where N and λ are state parameters defining the void ratio at σ'_v = 1 kPa and the slope of the normal compression line (NCL) at high levels of σ'_v, respectively. The over-consolidation ratio, OCR is defined as the ratio of the maximum vertical effective stress experienced by the soil, $\sigma'_{v,max}$, over the equilibrium vertical effective stress, $\sigma'_{v,eqm}$ where $\sigma'_{v,max}$ is the sum of the in situ self-weight vertical effective stress and additional soil surcharge pressure ($\sigma'_{v,max} = \sigma'_{v0} + \sigma'_{v,sur}$).

A curved NCL is considered (**Fig. 2(a)**) which accounts for the additional void ratio at low levels of vertical stress. This feature is required to match the experimental data shown later, and follows the model defined by Liu & Carter (2003). The additional void ratio at low levels of σ'_v is represented by the last term on the right-hand side of **Equation 2**, where Δe_i is the additional void ratio at $\sigma'_v = \sigma'_{v,i}$ where virgin yielding begins at effective stress, $\sigma'_{v,i}$. Power b_{NCL} quantifies the rate of increase of void ratio with decreasing σ'_v.

The initial CSL in e - ln(σ'_v) space (**Fig. 2(a)**) is a curved line parallel to the NCL, defined by the initial spacing ratio, R_0, given by the ratio of vertical stresses on the NCL and the initial CSL in e - ln(σ'_v) space:

$$R_0 = \exp\left(\frac{\mathrm{N} - \Gamma_0}{\lambda - \kappa}\right) \tag{3}$$

At any void ratio, e, the corresponding vertical effective stress on the CSL, $\sigma'_{v,CSL}$ can be calculated from **Equation 4**:

$$e = \Gamma - \lambda \ln\left(\sigma'_{v,CSL}\right) + \kappa \ln\left(OCR\right) + \left(1 - k_R\right)\Delta e_i \left(\frac{\sigma'_{v,i}}{R\sigma'_{v,CSL}}\right)^{b_{NCL}} \tag{4}$$

The spacing ratio, R and parameter k_R in **Equation 4** concurrently increase with cycles of shearing, which causes the CSL to migrate to a lower void ratio with increasing cycles to represent cyclic densification, as introduced later in sub-section (**e**).

(b) *Undrained shear strength*

The undrained shear strength, s_u, of a soil element is mobilised when the stress state reaches the CSL, and is calculated from the vertical effective stress at failure via a strength parameter, M (**Figs. 2(b), 3(b)**):

$$s_u = 0.5M\sigma'_v \tag{5}$$

The distribution of the current shear strength with depth can therefore be derived from the current void ratio through:

$$s_u = 0.5M \exp\left(\frac{\Gamma - e}{\lambda}\right) \tag{6}$$

(c) *Mobilised shear stress*

Cycles of surface shearing mobilise a shear stress, τ_{op} at the soil surface, with magnitude diminishing with depth (**Fig. 3(c)**). The mobilised shear stress will be controlled by the weakest 'slice' of soil in the one-dimensional column, with both s_u and τ varying with depth. For most practical soil strength profiles which have s_u increasing with depth, failure will occur at the soil surface, but strictly τ_{op} is controlled by:

$$\tau_{op} = \min\left(\frac{s_u}{I_\tau}\right) \tag{7}$$

between $z = 0$ and ∞.

The mobilised shear stress at depth z can then be determined as $\tau = I_\tau \tau_{op}$ where I_τ is the influence factor defining the distribution of shear stress with depth.

(d) *Equivalent cycle number*

For a soil element that fails during each cycle of shear stress, the cycle number is simply equal to the number of shear stress reversals. However, for soil elements that mobilise only a fraction of the undrained strength during a cycle, an equivalent number of cycles is defined, ΔN_{eq}, to allow these 'partial' cycles to be accumulated (**Fig. 3(d)**):

$$\Delta N_{eq} = \left(\frac{\tau}{s_u}\right)^{\chi} \tag{8}$$

Since ΔN_{eq} varies with depth, each soil layer possesses a different total of equivalent cycles, which reduces with increasing depth.

The power χ controls the non-linearity of equivalent cycle number with the stress ratio, τ/s_u, and is expected to be greater than unity, implying an escalating rate of 'damage' the closer the shear stress is to the soil strength.

Selection of an appropriate value for χ is presented in the section on calibration and derivation of model parameters.

(e) ***CSL migration based on shearing cycles***

A limitation of the basic critical state models such as Original and Modified Cam Clay is that the progressive densification that results from multiple cycles of shearing to the critical state is not captured. In the present study, to overcome this limitation, the critical state line migrates to a lower void ratio as a function of the number of equivalent cycles experienced. This concept is achieved by defining a progressive increase in the spacing ratio, R, with cycles of shearing (**Fig. 3(e)**). The spacing ratio is assumed to increase from the initial value of R_0 towards a limiting value, R_f, according to:

$$R = R_0 + \left(R_f - R_0\right) \cdot k_R \tag{9}$$

where R_0 is calculated from the critical state parameters and the in situ stresses in the virgin soil (defined later in **Eq. (27)**)) and R_f is determined from the initial spacing ratio and soil sensitivity defined by a cyclic T-bar test (**Eq. (28)**). The parameter k_R depends on the number of cycles (or equivalent cycles – **Eq. (8)**) of failure previously imposed on the soil element:

$$k_R = 1 - \exp\left(-3\frac{\sum \Delta N_{eq}}{N_{eq(95)}}\right) \tag{10}$$

where $\sum \Delta N_{eq}$ provides the current equivalent cycle number and $N_{eq(95)}$ is a parameter controlling the rate of migration of the CSL, equal to the number of cycles required for 95% of the migration of the current CSL to the final location. The selection of a value of $N_{eq(95)}$ is presented later, with the case study for the sliding foundation.

(f) ***Generation of excess pore pressure***

The excess pore pressure mobilised when a soil element is sheared to failure (**Fig. 3(f)**) is given by:

$$\Delta u_{e,\max} = \sigma'_v - \sigma'_{v,CSL} \tag{11}$$

where σ'_v is the current (pre-shearing) vertical effective stress. During the first shearing cycle, $\sigma'_v = \sigma'_{v,eqm}$ (**Eq. 1**), while during subsequent shearing cycle, σ'_v is calculated as:

$$\sigma'_v = \sigma'_{v(N-1)} + \Delta u_{e,dis} - \Delta u_{e,gen} \tag{12}$$

where $\sigma'_{v(N-1)}$ is the (pre-shearing) vertical effective stress of the preceding cycle, and $\Delta u_{e,dis}$ is the dissipated excess pore pressure during the current reconsolidation cycle (to be defined later).

The generated excess pore pressure, $\Delta u_{e,gen}$ is given by:

$$\Delta u_{e,gen} = \Delta u_{e,\max} \cdot \left(\frac{\tau}{s_u}\right)^{\beta} \tag{13}$$

The parameter β represents the curvature of the σ'_v - τ effective stress path created by the generated excess pore pressure, $\Delta u_{e,gen}$. For $\beta = 1$ the stress path is linear, but $\beta > 1$ is more typical, reflecting the shape of the stress path derived from Cam clay-type models, as shown schematically in **Fig. 2(b)**.

(g) ***Dissipation of excess pore pressure***

The degree of consolidation, U (based on settlement, rather than pore pressure dissipation), after shearing during a reconsolidation period can be estimated through a normalised time-settlement response of the form:

$$U = 1 - \frac{1}{1 + \left(\frac{T}{T_{50}}\right)^m} \tag{14}$$

In the present analysis, U is inferred from a solution based on elasto-plastic finite element analysis of a boundary value problem (e.g. Gourvenec & Randolph (2010), Gourvenec *et al.* (2014), Feng & Gourvenec (2015) for shallow foundations, or Chatterjee *et al.* (2012) and Chatterjee *et al.* (2013) for pipelines). It is assumed that the global dissipation rates identified in these previous studies provide adequate approximations of the pore pressure dissipation at element level within the one-dimensional model used in the present study.

In **Eq. 14,** the parameter T_{50} refers to the dimensionless time factor for 50 % of the consolidation settlement, w to occur (i.e. $U = \Delta e/\Delta e_{U=1} = 0.5$ where Δe is the change in void ratio within a consolidation cycle, and $\Delta e_{U=1}$ is the reduction in current void ratio when full consolidation takes place within a cycle such that when $t \rightarrow \infty$, U = 1 as defined below), and m is a constant. The dimensionless time, T is expressed as:

$$T = \frac{c_{ref}\, t}{d^2} \tag{15}$$

where t is the reconsolidation period, and d is drainage length (depending on the dimension of the infrastructure, typically taken as the foundation breadth, B or pipe diameter, D). The current operative coefficient of consolidation, c_{ref} can be obtained as:

$$c_{ref} = \alpha\left(k(1+e)\frac{\sigma'_{v,CSL}}{\lambda\gamma_w} \right) \tag{16}$$

where α is a factor to account for the anisotropic dissipation of pore water pressure during consolidation (Cocjin *et al.*, 2014), and k is the coefficient of soil permeability which can be expressed as a function of void ratio as:

$$k = a\left(\frac{e^b}{1+e} \right) \tag{17}$$

with a and b being fitting parameters to estimate the permeability-void ratio relationship of the soil (Sahdi, 2013).

The reduction in the current void ratio during a reconsolidation cycle for an equivalent degree of consolidation, U (**Fig. 3(g)**) is equivalent to $\Delta e = \Delta e_{U=1} \cdot U$, where $\Delta e_{U=1}$ can be obtained as:

$$\Delta e_{U=1} = \kappa \ln\left(\frac{\sigma'_{v(N-1)}}{\sigma'_{v(N-1)} - \Delta u_{e,gen}} \right) \tag{18}$$

During reconsolidation, the vertical effective stress increases by an amount equivalent to the dissipated excess pore pressure, which is given by (**Fig. 3(g)**):

$$\Delta u_{e,dis} = \left[\exp\left(\frac{\Delta e}{\kappa} \right) - 1 \right]\left(\sigma'_{v(N-1)} - \Delta u_{e,gen} \right) \tag{19}$$

This completes the calculations for a given cycle of shearing and reconsolidation, and the current void ratio, e is updated by Δe through **Eq. 18**, leading to a revised undrained strength, s_u, (**Eq. 6**) to be used for the next cycle computation.

(h) ***Change in soil height and surface settlement***

As the cycles progress, accumulating change in void ratio allows the change in height of each soil element with height, dz (**Fig. 3(h)**) to be determined as:

$$\delta h = \frac{\Delta e}{1+e} dz \tag{20}$$

Equation 20 is integrated over the whole depth of the soil column to obtain the incremental settlement of the soil surface within a cycle of reconsolidation,

$$\delta w = \int_{z=0}^{\infty} \delta h dz \tag{21}$$

where the current settlement of the soil surface, w, is obtained by summing δw for the current number of cycles N,

$$w = \sum_{1}^{N} \delta w \tag{22}$$

5. COMPARISON OF THEORETICAL FRAMEWORK AND MODEL TEST DATA

The proposed framework has been applied to centrifuge test results reported by Cocjin *et al.* (2014). The sliding resistance and settlement of a rectangular mat foundation on normally-consolidated clay is analysed, as well as changes in the strength of the underlying soil. Pertinent details of the centrifuge model testing and calibration of the framework parameters are outlined below.

Foundation test

The centrifuge test was conducted in the University of Western Australia – Centre for Offshore Foundation Systems (UWA – COFS) fixed beam centrifuge at an acceleration level of 100$\boldsymbol{g}$.

The rectangular model foundation (**Fig. 4**) (with dimensions B = 5 m and L = 10 m at prototype scale) was set down on the surface of a bed of normally consolidated kaolin clay and subjected to cycles of undrained sliding with periods of intervening consolidation. An operative vertical stress σ_{op} = 1.85 kPa (equivalent to an operative vertical load, V_{op} = 92.7 kN) was imposed by the model foundation throughout the test. The soil was allowed to consolidate fully under this stress prior to the cycles of sliding and consolidation. The loading sequence prescribed in the centrifuge test is illustrated in **Fig. 5**. The foundation was translated horizontally a distance δu = 0.5B at a rate of 1 mm/s, which was sufficiently rapid to maintain undrained conditions during the slide. A single slide (which occurred only once at the start of the sliding cycles), or a double slide (reverse and forward without intervening consolidation) is defined as a single cycle. The consolidation period after each movement lasted t = 1.5 years at prototype scale, during which the foundation was prevented from moving horizontally but was free to settle under the applied σ_{op}.

The foundation sliding resistance and settlements were recorded over cycles of horizontal sliding and intervening periods of consolidation, totalling more than 60 years (prototype scale) of foundation response.

Stress distribution

The influence factors for the vertical stress, I_σ and shear stress, I_τ distribution beneath the centreline of a rectangular, uniformly loaded area on the surface of a semi-infinite mass (Holl, 1940) were adopted, given by:

$$I_\sigma = \frac{2}{\pi}\left\{\tan^{-1}\left[\frac{lb}{zr_3}\right] + \frac{lbz}{r_3}\left[\left(\frac{1}{r_1}\right)^2 + \left(\frac{1}{r_2}\right)^2\right]\right\} \tag{23}$$

$$I_\tau = \frac{2}{\pi}\left\{\tan^{-1}\left[\frac{lb}{zr_3}\right] - \frac{lbz}{r_1{}^2 r_3}\right\} \tag{24}$$

where l = 0.5L and b = 0.5B with $L > B$. The parameters r_1, r_2, and r_3 are given as follows:

$$\begin{aligned} r_1 &= \left(l^2 + z^2\right)^{0.5} \\ r_2 &= \left(b^2 + z^2\right)^{0.5} \\ r_3 &= \left(l^2 + b^2 + z^2\right)^{0.5} \end{aligned} \tag{25}$$

Calibration and derivation of model parameters

Appropriate parameter values for the application of the theoretical framework were drawn from auxiliary tests carried out during the sliding foundation tests in the centrifuge as reported in Cocjin *et al.* (2014). **Table 1** provides a list of these model parameters and corresponding calibrated values used in the application of the theoretical model.

Critical state parameters

The critical state parameters λ, κ and N were calibrated from the moisture content profile of the centrifuge model soil sample.

The moisture content, m_c at different depths was obtained from vertical core samples taken from undisturbed sites of the centrifuge soil sample. This was used to calculate the effective unit weight of the soil as $\gamma' = \gamma_w(G_s-1)/(1-e_0)$ where $e_0 = m_cG_s$ is the in situ void ratio, and γ_w is the unit weight of water. The specific particle density, $G_s = 2.6$ (Stewart, 1992) yielded an average effective unit of $\gamma'_{av} = 6.0$ kN/m^3 over the range $0.4 < z$ (m) < 11.5.

The in situ void ratio, i.e. in the virgin soil prior to placement or loading of the foundation, e_0, and the natural logarithm of the vertical effective stress, $\sigma'_{v0} = \gamma'_{av}\cdot z$ representing undisturbed soil are presented in **Fig. 6**. The measured data show higher in situ void ratios at low stress levels ($\sigma'_{v0} < 10$ kPa) than predicted by critical state parameters derived from one-dimensional compression tests at higher stresses (Stewart, 1992). This reflects the high compressibility of clays with high initial water contents (Boukpeti *et al.*, 2012) and justifies our use of a modified shape of NCL and CSL, following Liu & Carter (2003).

By minimising the residuals between the measured and predicted void ratio from **Eq. 2**, best-fit values for the slopes, λ and κ, and void ratio intercept at $\sigma'_v = 1$ kPa, N, and additional void ratio parameters Δe_i, $\sigma'_{v,i}$ and b_{NCL}, were obtained (**Table 1**).

The value of the void ratio intercept at $\sigma'_v = 1$ kPa of the initial CSL in the $\ln(\sigma'_v) - e$ plane, Γ_0 was obtained by equating the ratio of the in situ undrained shear strength (**Eq. 6**) and the effective vertical stress at the NCL (**Eq. 2**), with the normally consolidated strength ratio of the soil, $(s_u/\sigma'_{v0})_{NC}$ such that

$$\Gamma_0 = \lambda \ln\left[\frac{2}{M}\left(\frac{s_u}{\sigma'_{v0}}\right)_{NC}\right] + \mathrm{N} \tag{26}$$

Spacing ratio

The initial spacing ratio, R_0, is expressed as a function of the normally consolidated strength ratio by substituting **Eq. 26** into **Eq. 3**:

$$R_0 = \exp\left[\left(\frac{\lambda}{\kappa-\lambda}\right)\ln\left(\frac{2}{M}\left(\frac{s_u}{\sigma'_{v0}}\right)_{NC}\right)\right] \tag{27}$$

wherein the obtained R_0 (**Table 1**) is derived from an $(s_u/\sigma'_{v0})_{NC} \sim 0.15$ reported in Cocjin *et al.* (2014) from T-bar penetrometer tests, assuming $M = 0.92$ following Stewart (1992).

The final spacing ratio, R_f, which defines the limiting position of the CSL in the volumetric plane, was obtained from the measured soil sensitivity through cyclic T-bar penetrometer tests, $S_t \sim 2.4$ (Cocjin *et al.*, 2014) as:

$$R_f = R_0 S_t \tag{28}$$

Remoulding parameter

The variation of the change in equivalent cycle number ΔN_{eq} caused by the mobilised stress ratio, τ/s_u is illustrated in **Fig. 7** for different values of χ. The parameter χ controls the level of 'damage' for non-failing soil elements as quantified in **Eq. 8**. A choice of $\chi > 1$ reflects a realistic assumption regarding the level of 'damage' for non-failing soil elements as a function of the mobilised stress ratio, τ/s_u. A very large χ would limit significant 'damage' only to a soil element that has reached the critical state failure, whereas a linear variation of the level of 'damage' with τ/s_u is implied by $\chi = 1$. As χ controls the fraction of the full pore pressure that is generated during shearing without failure, the τ/s_u versus ΔN_{eq} representation (as shown in **Fig.7**) might be expected to resemble a mirror image of the effective stress path in (σ'_v, τ) space. For soft clays this path bends to the left, and is approximately elliptical (e.g. as in Modified Cam Clay). The adopted value of $\chi = 2.5$ approximates this well, and might therefore be expected to apply more generally, as well as fitting the present experimental data.

Similarly, by using $\beta = 2$ in **Eq. 13**, a parabolic form is adopted for the curvature tracked by the generated excess pore pressure, $\Delta u_{e,gen}$ in (σ'_v, τ) space (**Fig. 2(b)**). A value of $N_{eq(95)} = 40$ provided a good match with the observed data.

Assessment of the theoretical model

This section compares the results from the framework with observations from the centrifuge model test reported in Cocjin *et al.* (2014).

Foundation sliding resistance

Figure 8 compares the horizontal sliding resistance calculated by the framework (via **Eq. 7**) and measured in the centrifuge test. The model captures well the general trend and magnitude of increasing sliding resistance due to increasing soil strength following cycles of shearing and reconsolidation. A residual coefficient of sliding friction, $\mu = \tau_{op}/\sigma_{op}$ is calculated at every sliding cycle where τ_{op} obtained from the centrifuge test refers to the residual, steady state, shear stress mobilised at a horizontal foundation displacement of $\delta u/B = 0.25$. The test results showed a declining sliding resistance during the later cycles ($N > 30$) which was not included in **Fig. 8**. This occurred because contact between the edge of the mudmat and the seabed was not maintained as the mudmat moved in to and out of the depression created by the consolidation process and onto the adjacent berm (see Cocjin *et al.*, 2014). Further work would be required to introduce this three dimensional behaviour into a theoretical model.

Foundation settlement

Figure 9(a) compares the calculated and measured accumulation of foundation consolidation settlement. The measured consolidation settlement in the early cycles is slightly greater than the calculations while the settlement in the later cycles and the final consolidation settlement are very well matched.

The final consolidation settlement was obtained from the measured initial and final void ratio profiles (**Fig. 6**) by summing the changes in soil height with depth. The settlement derived from the changes in void ratio is identical to the final cyclic consolidation settlement measured directly from the foundation test, providing confidence in the two independently calculated values (**Fig. 9(a)**).

The settlement of the foundation accumulates over a larger number of cycles than the rise in sliding resistance, which is virtually complete after 20 cycles (**Fig. 8**). This is due to continued pore pressure generation due to pre-failure shearing in the deeper soil, which leads to settlement but no change in the sliding resistance, which is controlled by the shallow soil. The framework correctly captures these different rates of resistance and settlement build-up with sliding cycles.

The sliding movement of the foundation also contributes plastic vertical displacement to the overall settlement, as evidenced from the centrifuge data in **Fig. 9(b),** which shows the overall cumulative foundation settlement against the horizontal sliding displacement, δu. The undrained shearing settlement, w_p is deducted from the overall cumulative foundation settlement in **Fig. 9(b)** and plotted against cycle number in **Fig. 9(a)**. This settlement is due to the ploughing of the sheared soil during sliding (Cocjin *et al.*, 2015), and is presented in **Fig. 10** as a plastic strain ratio, $\delta w_p/\delta u$ plotted against the normalised vertical load $v = V_{op}/V_{u,cons}$ where $V_{u,cons}$ is the consolidated, undrained vertical load capacity calculated from the updated soil strength following Gourvenec *et al.* (2014).

An associated flow rule was considered for prediction of the plastic settlement, but the actual response is non-associated, with higher settlement observed than predicted using normality combined with the failure envelopes for rectangular surface foundations by Feng *et al.* (2014) and the classical solution for a strip foundation by Green (1954). This is consistent with previous model test observations reported by Martin & Houlsby (2001), who applied an ad hoc scaling to the flow rule to capture non-associativity in their model tests of foundations on clay. In the present case, a simple relationship between the plastic strain direction and the normalised vertical load derived from the centrifuge data in **Fig. 10** is given as:

$$\frac{\delta w_p}{\delta u} = \Lambda\left(v - v_0\right)^{\xi} \text{ for } v > v_0, \tag{29a}$$

and

$$\frac{\delta w_p}{\delta u} = 0 \text{ for } v \leq v_0 \tag{29b}$$

where Λ and ξ are fitting parameters (see **Table 2**), and v_0 is the lowest vertical load ratio with non-zero plastic strain. The cut-off of $v_0 = 0.27$ is lower than the theoretical value derived from failure envelopes (0.4 and 0.5 in Feng *et al.* (2014) and Green (1954), respectively).

Undrained shear strength profiles

Figure 11 shows a good correlation between the in situ undrained shear strength in the virgin soil, $s_{u,0}$ profile measured in the centrifuge sample with a miniature T-bar test (Stewart & Randolph, 1991) and calculated by the framework through **Eq. 6**.

A T-bar test was also carried out in the foundation footprint, after removal of the foundation at the end of the test, to assess the final undrained shear strength, $s_{u,f}$ of the sheared and consolidated soil. The profile of $s_{u,f}$, measured from the surface of the foundation footprint is compared with the calculations from the theoretical framework in **Fig. 11** and also shows good agreement (noting that the T-bar diameter corresponds to 0.5 m at prototype scale, so detection of the hardened zone is challenging).

Moisture content profiles

Figure 12 compares the in situ and final moisture content profiles with depth from the framework and measured in the centrifuge test sample. The framework result was derived from the cycle-by-cycle void ratio profile, where moisture content was obtained as $m_c = e/G_s$ for the first and last cycle. The framework provides a good estimate of the in situ moisture content profile of the centrifuge test sample, and a reasonable estimate of the lower post-test moisture content at shallow depth.

6. INSIGHTS INTO SOIL RESPONSE

The analysis framework has been shown to provide good predictions of the foundation resistance to sliding and settlement with cycles of shearing and consolidation, as well as capturing the changing undrained shear strength and moisture content of the underlying soil. The framework can also provide insights into the cycle-by-cycle elemental soil response as described below.

Void ratio

Figure 13 shows the cycle-by-cycle evolution of the profile of void ratio, e as a function of depth for 40 loading cycles. The general behaviour shows that during the early cycles, the greatest contraction is at the soil surface. However, as this zone hardens, the shear stress and pore pressure generation in the deeper soil increase, leading to a greater change in void ratio. This effect propagates deeper but diminishes as the mobilised shear stress becomes a smaller proportion of the in situ shear strength.

Undrained shear strength

Figure 11 is replotted in **Fig. 14** to show the cycle-by-cycle evolution of undrained shear strength, s_u (**Eq. 6**) as a function of depth showing the general increase in soil strength, over the depth of influence of pore pressure generation, with increasing cycles of surface shearing and reconsolidation. The undrained shear strength close to the surface reaches a limiting value after some cycles, while the zone of strength gain propagates deeper. This stabilisation of the strength reflects the final critical state being reached and the end of the CSL migration, leading to no further excess pore pressure.

Stress and state path

State paths during cycles of surface shearing and reconsolidation for a soil element at the shearing interface, i.e. at z = 0 is presented in e - ln(σ'_v) space for 40 loading cycles in **Fig. 15**. This figure shows the progressive reduction of vertical effective stress at constant void ratio within a surface shearing cycle, and the recovery of effective stress and associated reduction in void ratio during each reconsolidation period. The decay and migration of the CSL in e – ln(σ'_v) space becomes less pronounced with increasing cycles of shearing and reconsolidation. The effect of partial consolidation is also seen by the decreasing value of σ'_v from $\sigma'_{v,eqm}$ with increasing loading cycle.

7. CLOSING REMARKS

The analytical framework set out in this paper is an extension of the widely-used oedometer method for estimating foundation settlement. It provides a basis to predict the changing seabed resistance and accumulating settlements of surface installations that experience cycles of horizontal sliding movements.

The framework considers a one-dimensional column of soil elements beneath a foundation, with each element subject to a vertical total stress and cycles of horizontal shear stress, and responding via a simple form of critical state model. The framework is presented in a cycle-by-cycle manner, solving for the response at each soil element to determine the cumulative change in void ratio, defining changes in soil shear strength and surface settlement.

The change in undrained shear strength is quantified in terms of the generation and dissipation of excess pore water pressure. The model incorporates the effects of partial dissipation of excess pore water pressure during cycles of reconsolidation. Soil contraction due to void ratio reduction during cycles of reconsolidation allows for the estimation of soil surface settlement.

The framework was shown to simulate well the behaviour of a tolerably mobile subsea foundation tested at prototype stress levels in the centrifuge. The model captures the increasing foundation sliding resistance due to increasing soil strength, the overall settlement of the foundation following cycles of shearing and reconsolidation, as well as the different build-up rates of resistance and settlement. The theoretical model also provided an accurate estimate of the spatial variation with depth of the undrained shear strength and the moisture content of the soil within the foundation footprint.

This framework provides a simple yet effective means to analyse a soil-structure interaction process that involves episodes of horizontal surface shearing and reconsolidation. It is a simple tool that is convenient for foundation design purposes – validated for specific conditions, if necessary, via more complex model tests or numerical analysis. It also provides a simple method to integrate the foundation behaviour into a structural model that includes the connected equipment such as pipelines, without requiring the full soil domain to be modelled explicitly. It offers a useful addition to the toolbox of methods that can be used to design and optimise subsea installations.

8. ACKNOWLEDGEMENTS

This work forms part of the activities of the Centre for Offshore Foundation Systems (COFS), currently supported as a node of the Australian Research Council's Centre of Excellence for Geotechnical Science and Engineering, and through the Fugro Chair in Geotechnics, the Lloyd's Register Foundation Chair and Centre of Excellence in Offshore Foundations and the Shell EMI Chair in Offshore Engineering. The work presented in this paper is supported through ARC grant DP140100684.

9. REFERENCES

Andersen, K. H. (1976). Behaviour of clays subjected to undrained cyclic loading. In *Proceedings of International Conference on the Behaviour of Offshore Structures.* pp. 392-403.

Andersen, K. H. (2009). Bearing capacity under cyclic loading: offshore, along the coast, and on land. The 21st Bjerrum Lecture presented in Oslo, 23 November 2007. *Can. Geotech. J.* **46**, No. 5, 513–535.

Boukpeti, N., White, D. J., Randolph, M. F., & Low, H. E. (2012). Strength of fine- grained soils at the solid-fluid transition. *Géotechnique* **62**, No. 3, 213-226, http://dx.doi.org/10.1680/geot.9.P.069.

Chatterjee, S., White, D. J., & Randolph, M. F. (2013). Coupled consolidation analysis of pipe–soil interactions. *Canadian Geotechnical Journal* **50**, 609-619, http://dx.doi.org/10.1139/cgj-2012-0307.

Chatterjee, S., Yan, Y., Randolph, M. F., & White, D. J. (2012) Elastoplastic consolidation beneath shallowly embedded offshore pipelines. *Géotechnique Lett.* **2**, April – June, 73–79, http://dx.doi.org/10.1680/geolett.12.00031

Cocjin, M. L., Gourvenec, S. M., White, D. J., & Randolph, M. F. (2015). Effects of drainage on the response of a sliding subsea foundation. In *Proceedings of 3rd International Symposium on Frontiers in Offshore Geotechnics*. Oslo, pp. 777-782. London, UK: Taylor & Francis Group.

Cocjin, M., Gourvenec, S., White, D., & Randolph, M. (2014). Tolerably mobile subsea foundations – observations of performance. *Géotechnique* **64**, No. 11, 895–909, http://dx.doi.org/10.1680/geot.14.P.098.

Deeks, A., Zhou, H., Krisdani, H., Bransby, F. & Watson, P. (2014). Design of direct on-seabed sliding foundation. In *Proceedings of the 33rd International Conference on Ocean, Offshore and Arctic*

Engineering, San Francisco, USA, paper V003T10A024, http:// dx.doi.org/10.1115/OMAE2014-24393. New York, NY, USA: ASME.

Feng, X. & Gourvenec, S. (2016) Modelling sliding resistance of tolerably mobile subsea mudmats. *Géotechnique* **66**, No. 6, 490–499, http://dx.doi.org/10.1680/jgeot.15.P.178.

Feng, X., & Gourvenec, S. (2015). Consolidated undrained load-carrying capacity of subsea mudmats under combined loading in six degrees of freedom. *Géotechnique* **65**, No. 7, 563–575, http://dx.doi.org/10.1680/geot.14.P.090.

Feng, X., Randolph, M. F., Gourvenec, S., & Wallerand, R. (2014). Design approach for rectangular mudmats under fully three-dimensional loading. *Géotechnique* **64**, No. 1, 51–63, http://dx.doi.org/10.1680/geot.13.P.051.

Fisher, R. and Cathie, D. (2003). Optimisation of gravity based design for subsea applications. In *Proc. International Conference on Foundations (ICOF)*. Dundee, pp. 283–296.

France, J. W. & Sangrey, D. A. (1977). Effects of drainage in repeated loading of clays. *J. Geotech. Engng Div. ASCE* **103**, No. GT7, 769–785.

Gourvenec, S. & Randolph, M. F. (2010). Consolidation beneath circular skirted foundations. *International Journal of Geomechanics* **10**, No. 1, 22–29, http://dx.doi.org/10.1061/(ASCE)1532-3641(2010)10:1(22).

Gourvenec, S., Vulpe, C., & Murthy, T. (2014). A method for predicting the consolidated undrained bearing capacity of shallow foundations. *Géotechnique* **64**, No. 3, 215–225, http://dx.doi.org/10.1680/geot.13.P.101.

Green, A. P. (1954). The plastic yielding of metal junctions due to combined shear and pressure. *Journal of the Mechanics and Physics of Solids* **2**, No. 3, 197-211.

Hodder, M. S., White, D. J., & Cassidy, M. J. (2013). An effective stress framework for the variation in penetration resistance due to episodes of remoulding and reconsolidation. *Géotechnique* **63**, No. 1, 30–43, http://dx.doi.org/10.1680/geot.9.P.145

Holl, D. L. (1940). Stress transmissions in earths. *Proc. High. Res. Board*, Vol. 20, pp. 709-721.

Liu, M. D., & Carter, J. P. (2003). Volumetric Deformation of Natural Clays. *International Journal of Geomechanics*, **3**, No. 2, 236–252, http://dx.doi.org/10.1061/(ASCE)1532-3641(2003)3:2(236).

Martin, C. M. and Houlsby, G. T. (2001). Combined loading of spudcan foundations on clay: numerical modelling. *Géotechnique* **51**, No. 8, 687-699, http://dx.doi.org/10.1680/geot.2001.51.8.687.

Poulos, H. G. & Davis, E. H. (1974). *Elastic solutions for soil and rock mechanics*. New York: John Wiley & Sons, Inc.

Sahdi, F. (2013). *The changing strength of clay and its application to offshore pipeline design*. PhD thesis, The University of Western Australia, Perth, Australia.

Skempton, A.W. and Bjerrum, L. (1957). Contribution to the settlement analysis of foundations on clay. *Géotechnique* **7**, No. 4, 168–178.

Stewart, D. P. & Randolph, M. F. (1991). A new site investigation tool for the centrifuge. In *Proceedings of international conference on centrifuge modelling, Centrifuge '91*, Boulder (eds H.-Y. Ko and F. G. McLean), pp. 531–538. Rotterdam, the Netherlands: Balkema.

Stewart, D. P. (1992). *Lateral loading of piled bridge abutments due to embankment construction*. PhD thesis, The University of Western Australia, Perth, Australia.

White, D. J. & Hodder, M. (2010). A simple model for the effect on soil strength of episodes of remoulding and reconsolidation. *Can. Geotech. J.* **47**, No. 7, 821–826, http://dx.doi.org/10.1139/T09-137.

Xiao, Z., Tian, Y. & Gourvenec, S.M. (2016) A practical method to evaluate failure envelopes of shallow foundation considering soil strain softening and rate effects., *Applied Ocean Research*, **59**,: 395-407, http://dx.doi.org/10.1016/j.apor.2016.06.015..

Yan, Y., White, D. J. & Randolph, M. F. (2014). Cyclic consolidation and axial friction for seabed pipelines. *Géotechnique Lett.* **4**, July–September, 165–169, http://dx.doi.org/10.1680/ geolett.14.00032.

11. LIST OF FIGURES

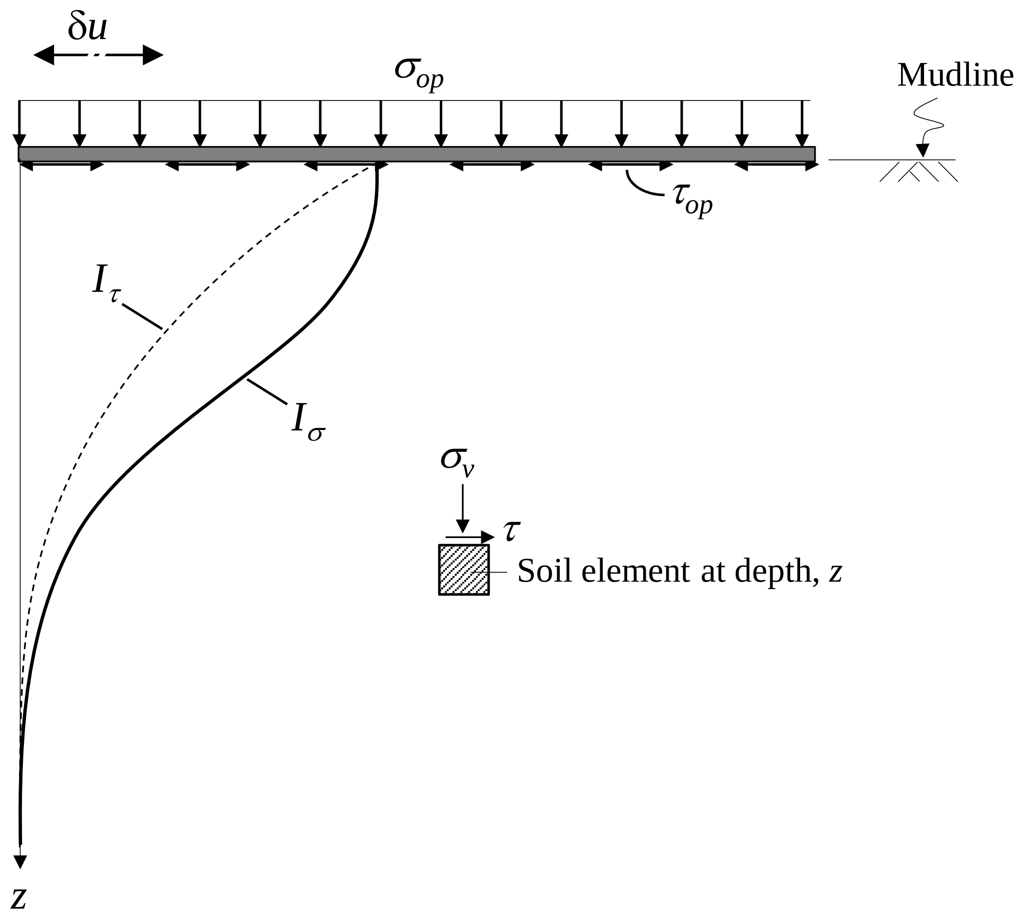

Figure 1. Idealisation of the boundary value problem showing distributed loads on the surface of a semi-infinite mass.

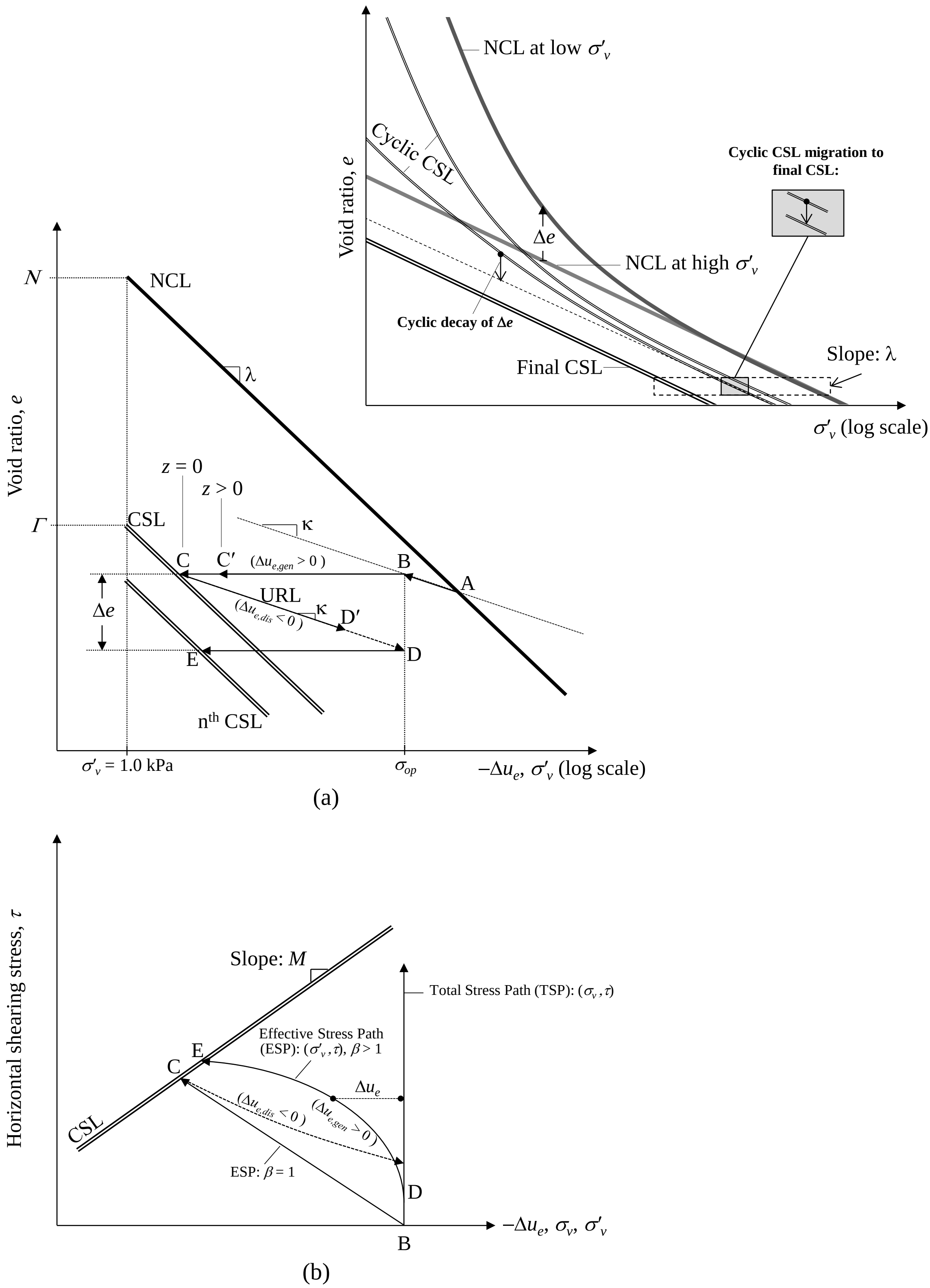

Figure 2. A critical state interpretation of a soil element submitted to cyclic surface shearing and reconsolidation, presented in the (a) volumetric (inset: migration and decay of critical state line), and (b) stress planes.

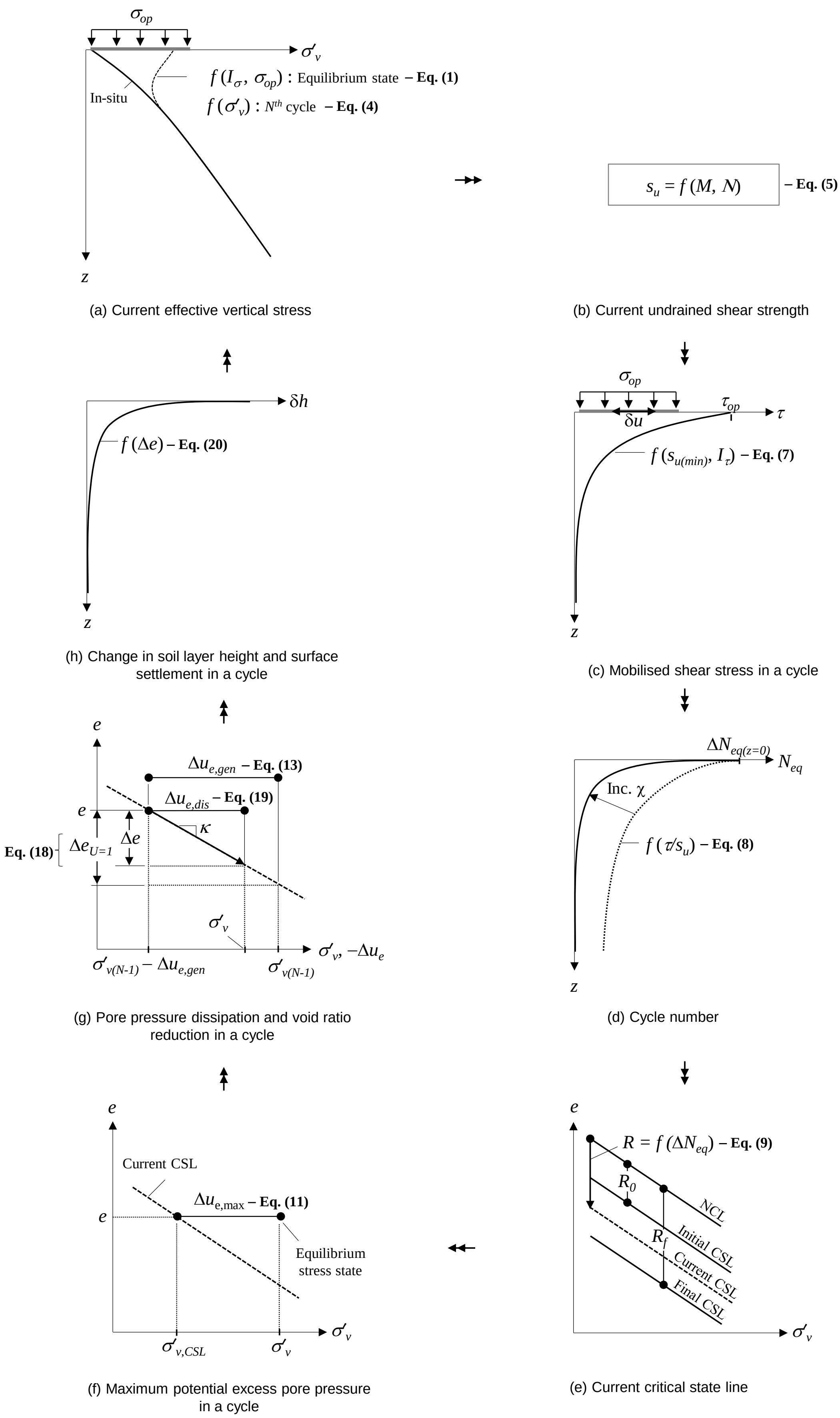

Figure 3. Schematic of model framework.

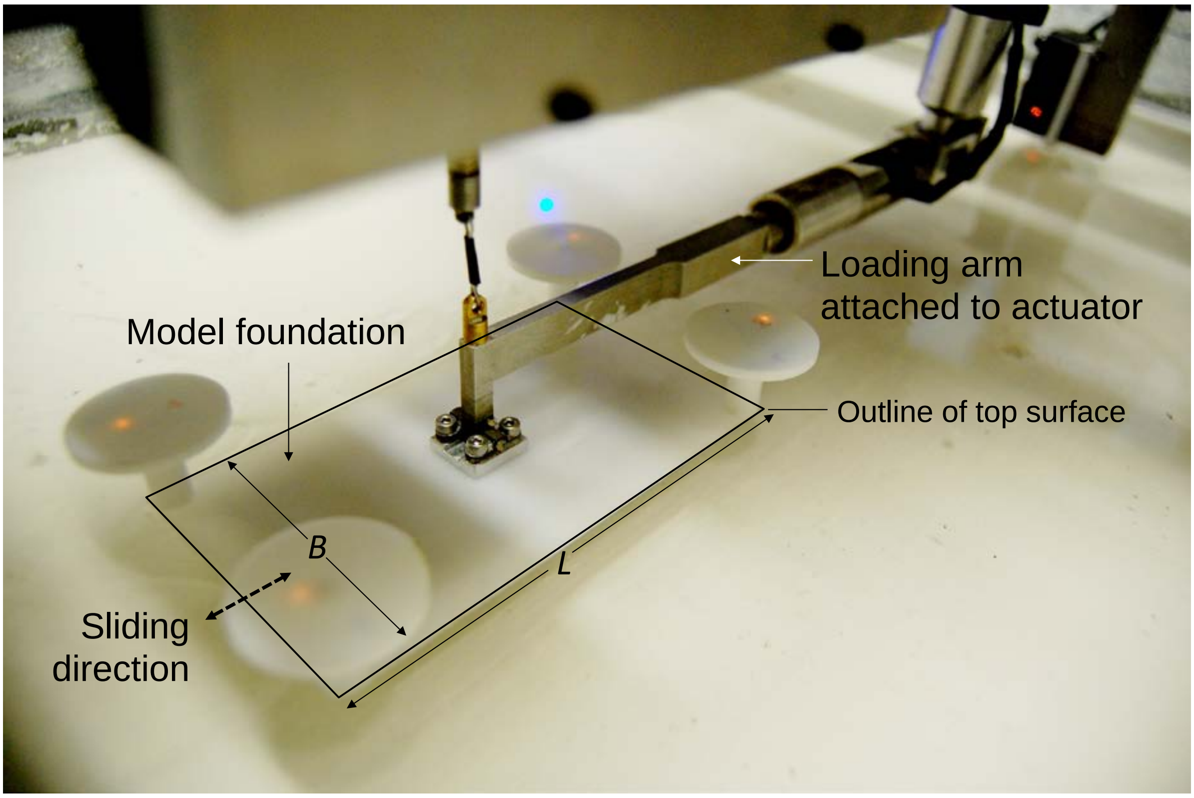

Figure 4. Experimental set-up of the sliding foundation test in the centrifuge.

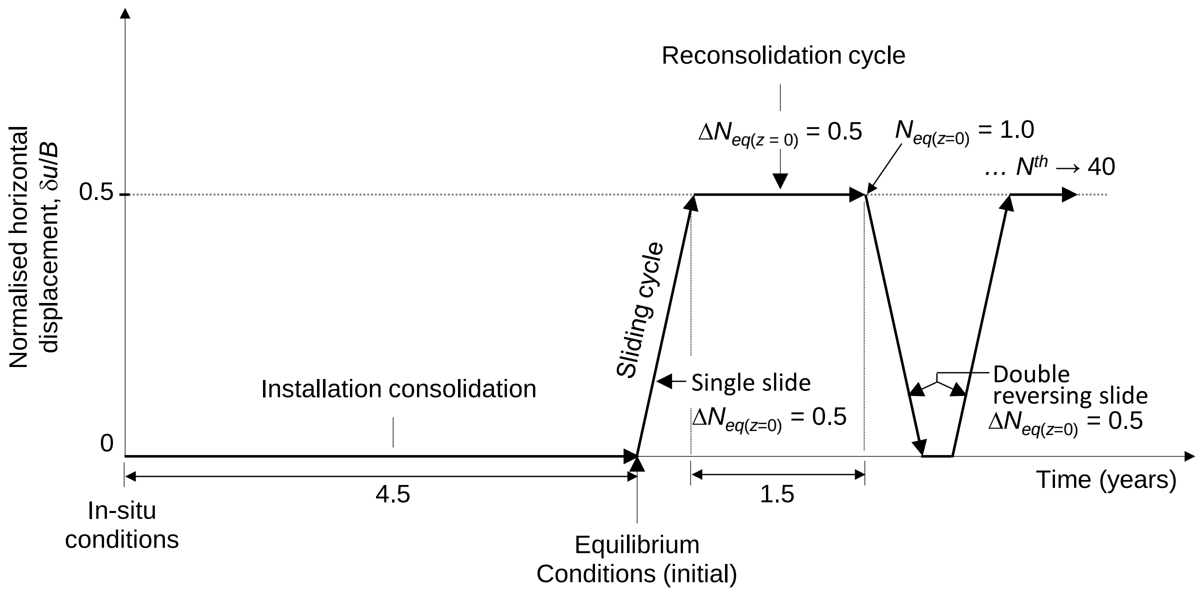

Figure 5. Loading sequence for a sliding foundation test in the centrifuge

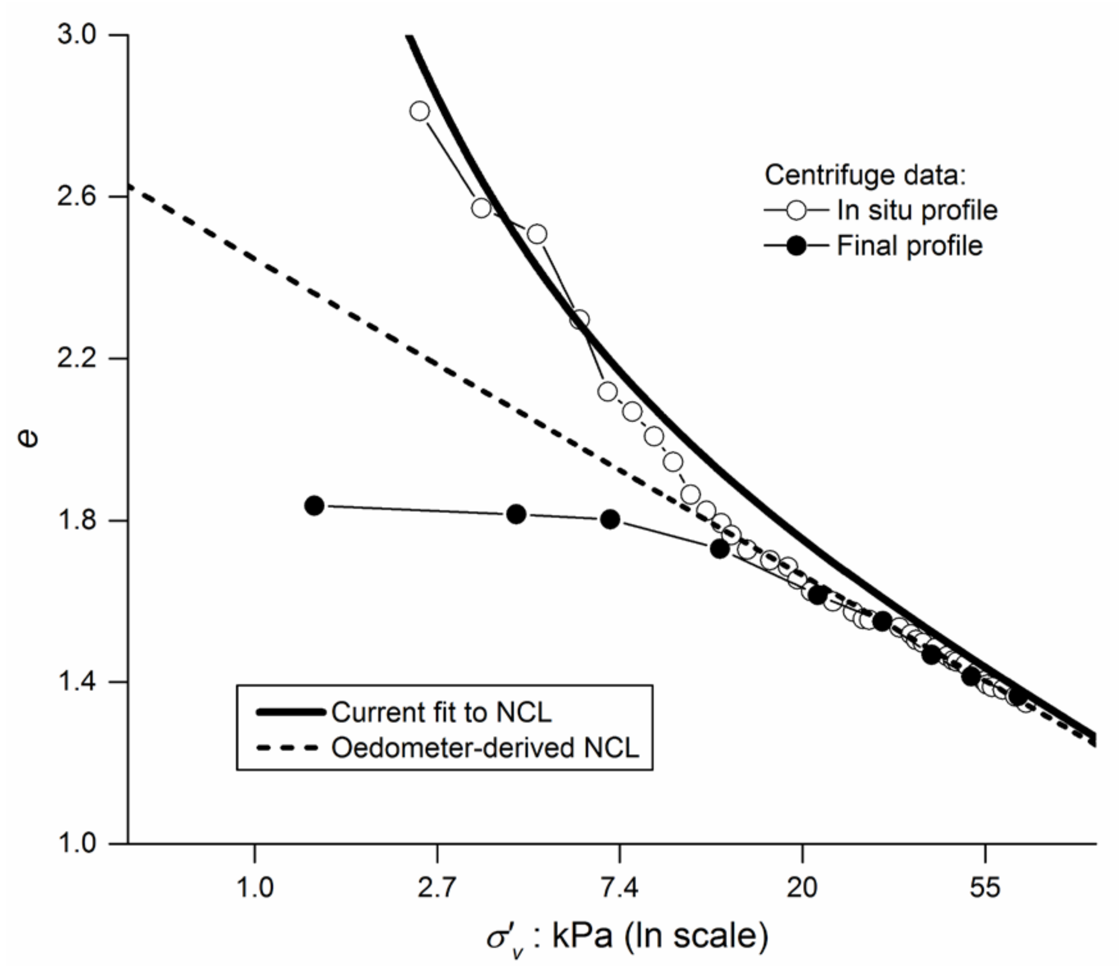

Figure 6. Vertical effective stress, σ'_v (in natural logarithm scale) plotted against void ratio, *e* showing measured data on in situ and sheared/consolidated soil (final), with linear models of the normal compression line (NCL) based on curve fits using state parameters obtained from the centrifuge, and one-dimensional compression tests.

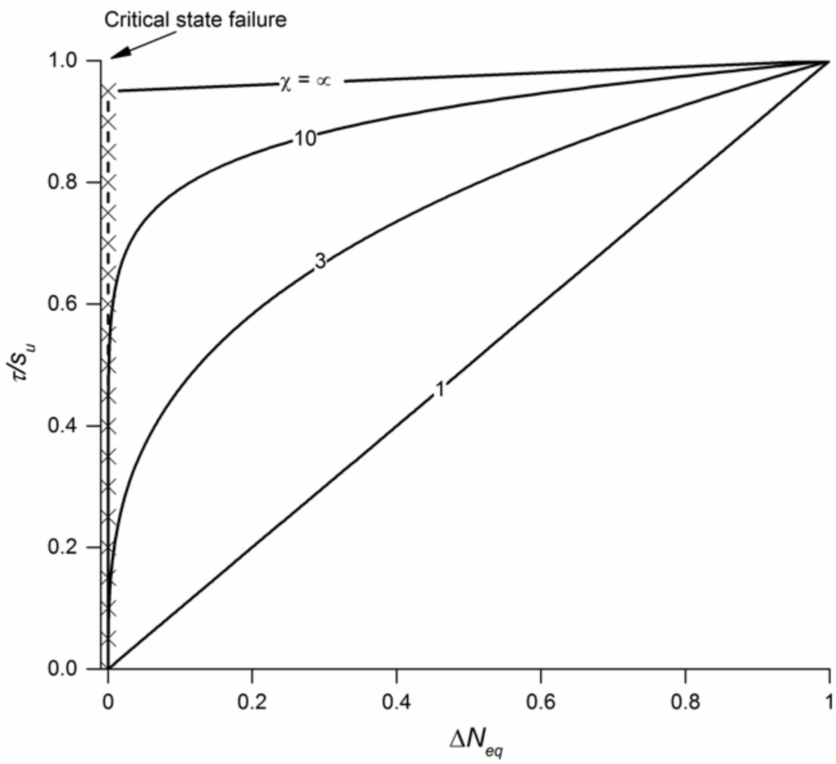

Figure 7. Variation of the change in cycle number ΔN_{eq} with mobilised stress ratio, τ/s_u for different values of χ.

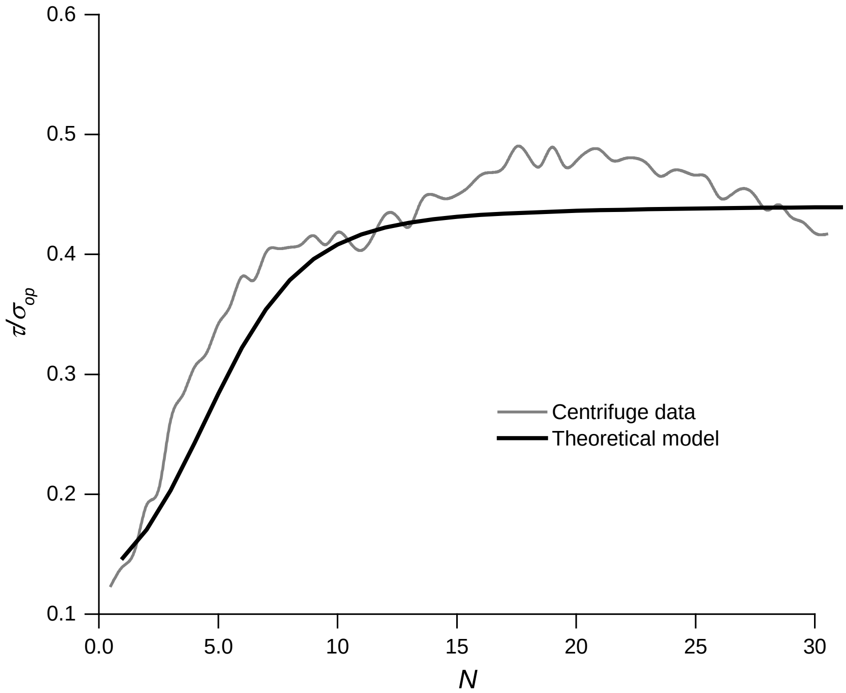

Figure 8. Residual coefficient of sliding friction, $\mu = \tau_{op}/\sigma_{op}$ mobilised at every loading cycle, measured from sliding foundation test in the centrifuge, and the prediction by the theoretical model.

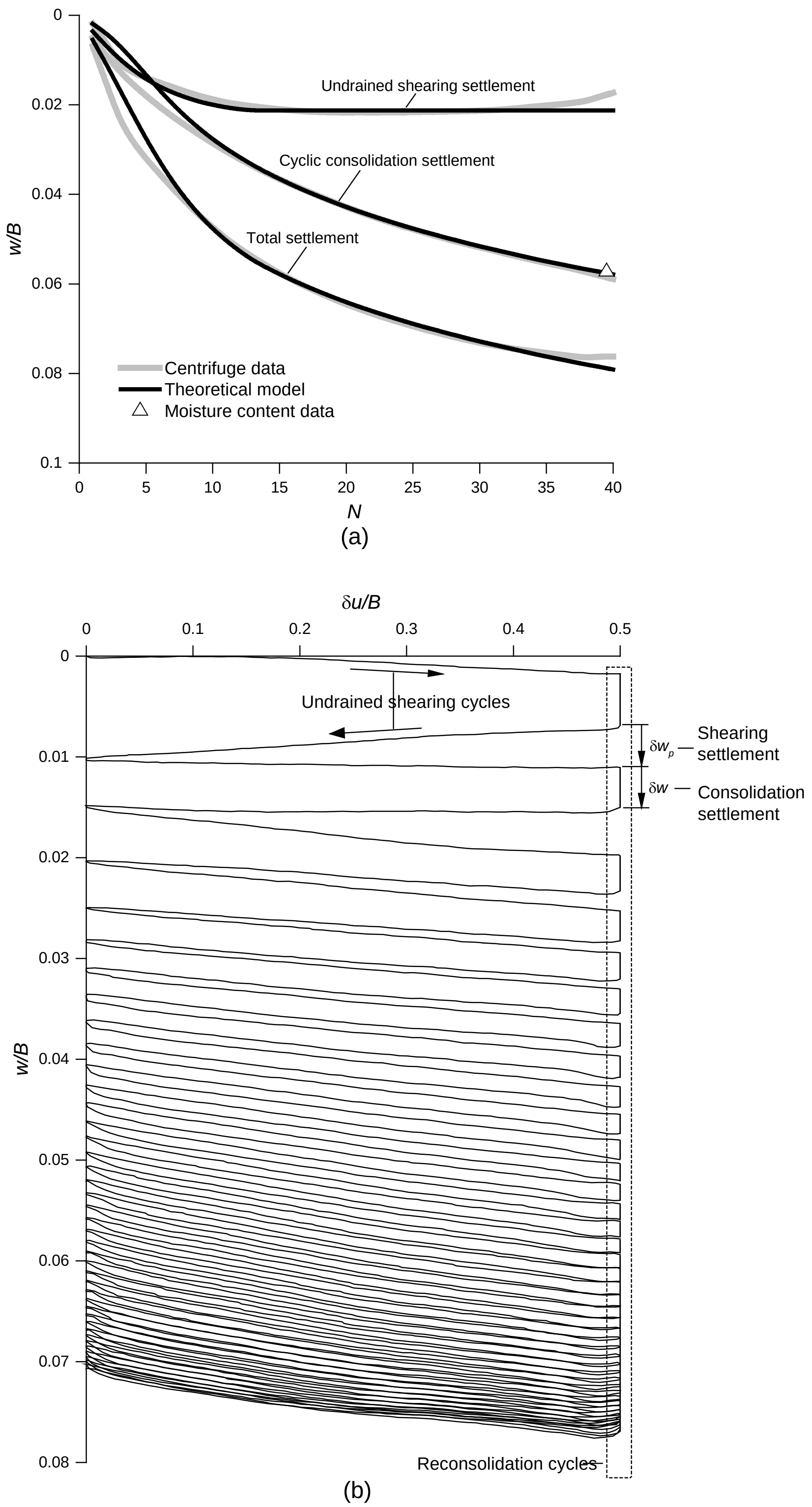

Figure 9. (a) accumulation of foundation settlement with increasing loading cycles, measured from sliding foundation test in the centrifuge, and the prediction by the theoretical model; and (b) overall foundation settlements measured in the centrifuge test.

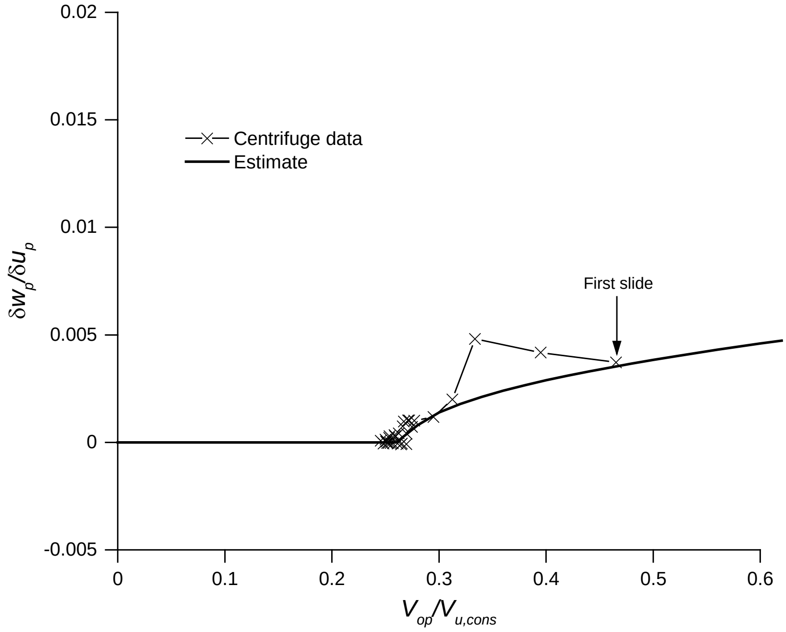

Figure 10. Incremental plastic undrained settlements.

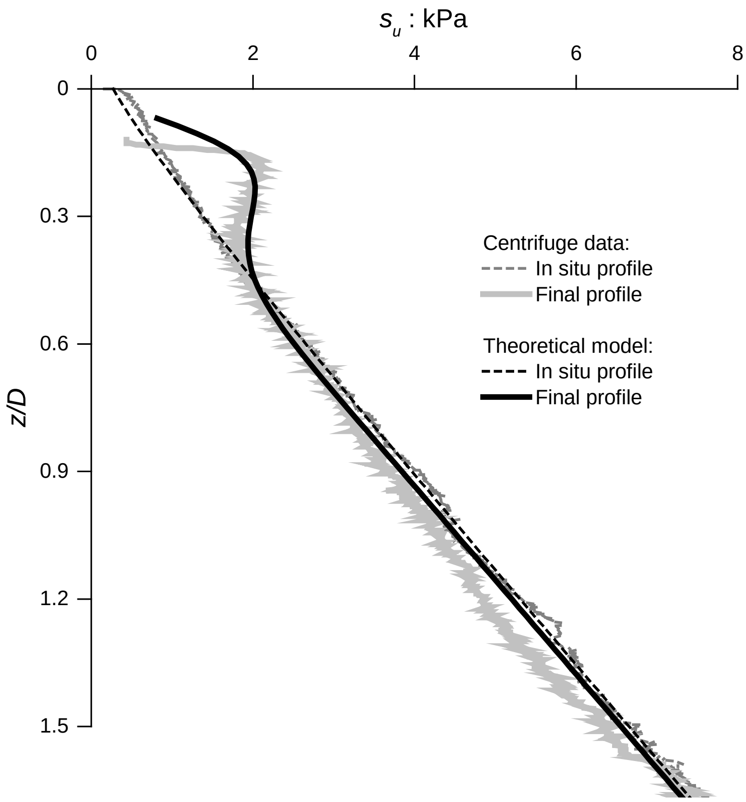

Figure 11. In situ and sheared/consolidated soil (final) undrained shear strength profiles with depth measured from the centrifuge test soil sample, and the prediction by the theoretical model.

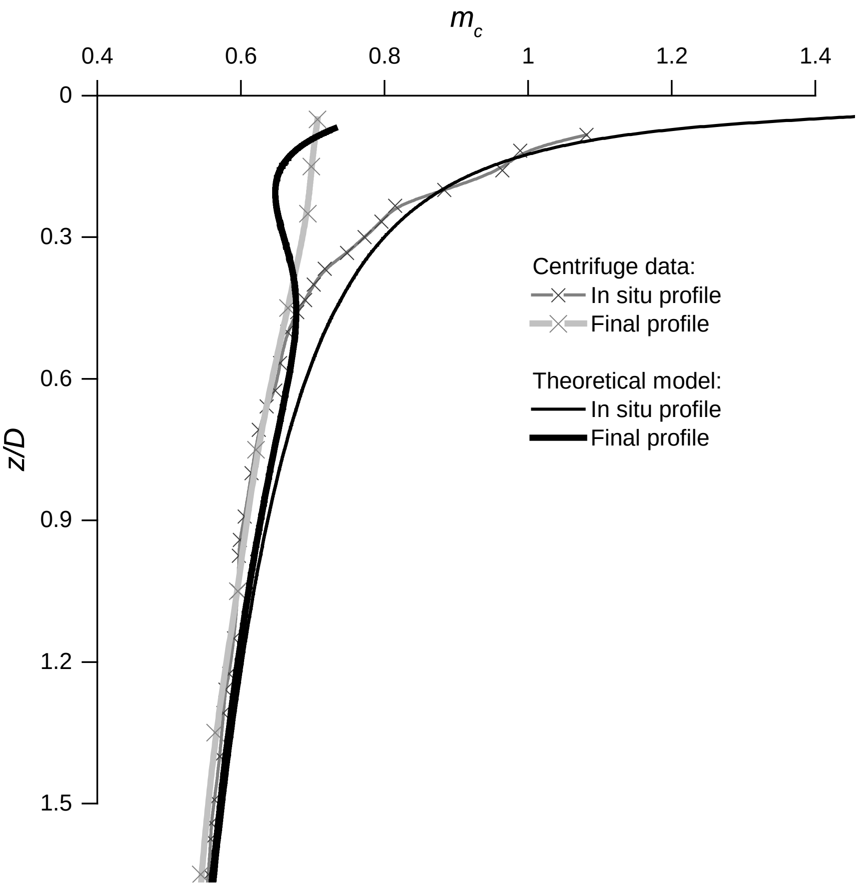

Figure 12. Moisture content, m_c profile with depth measured from the centrifuge test soil sample, and the prediction by the theoretical model.

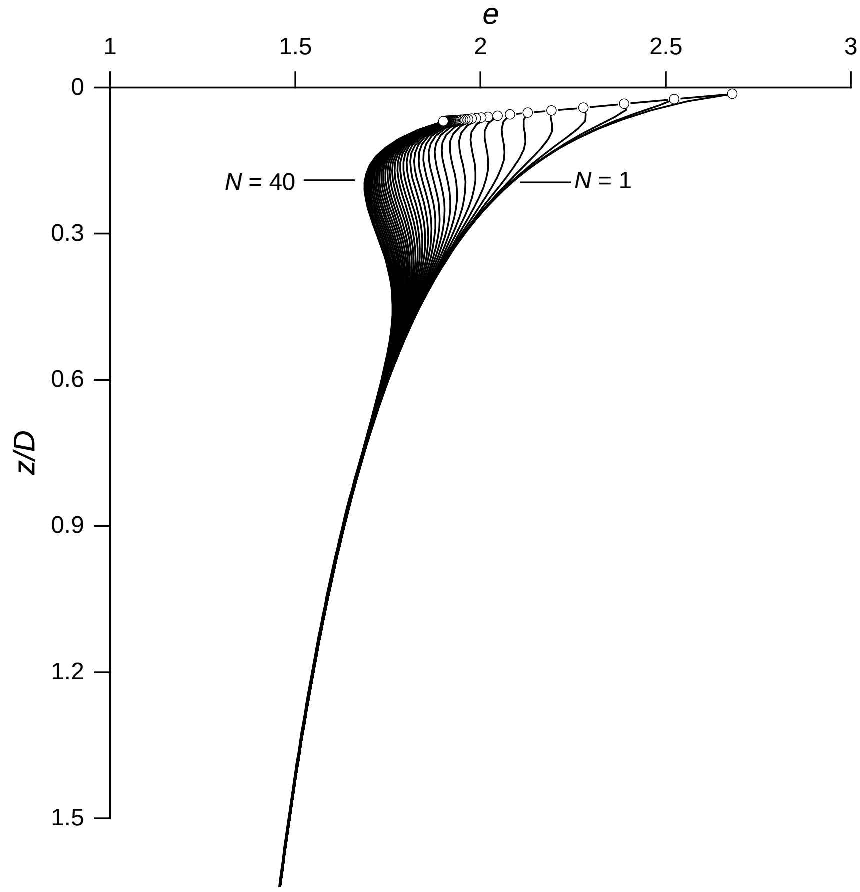

Figure 13. Cycle-by-cycle evolution of the current void ratio, *e* as a function of depth reflecting the degradation of the mudline level

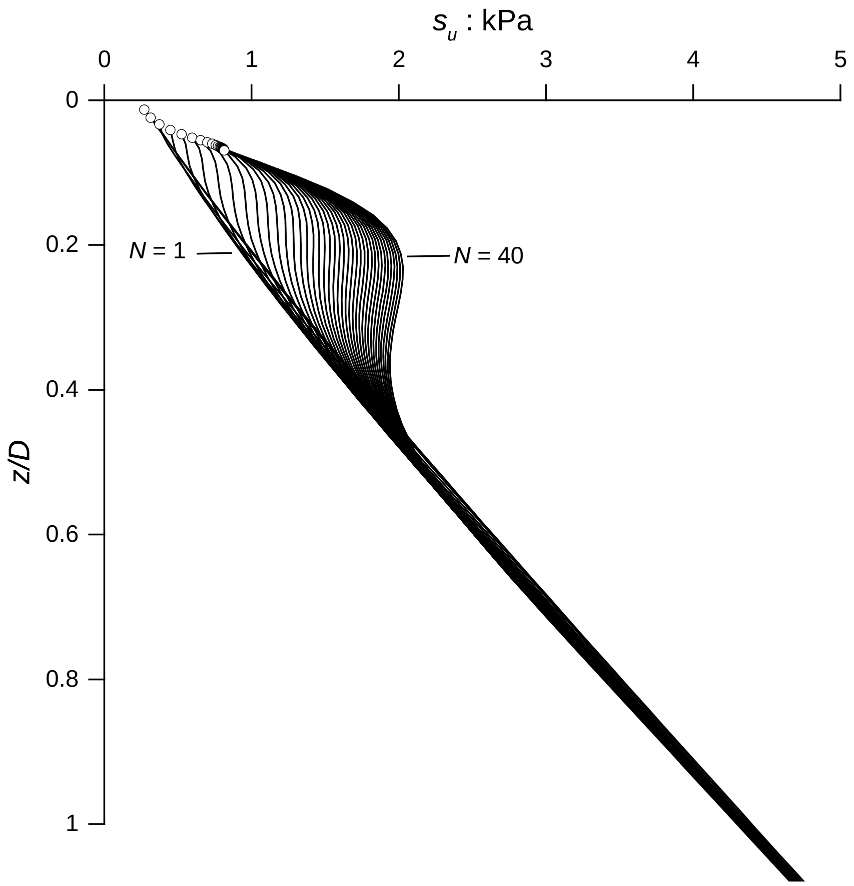

Figure 14. Cycle-by-cycle evolution of the current undrained shear strength, s_u as a function of depth reflecting the degradation of the mudline level

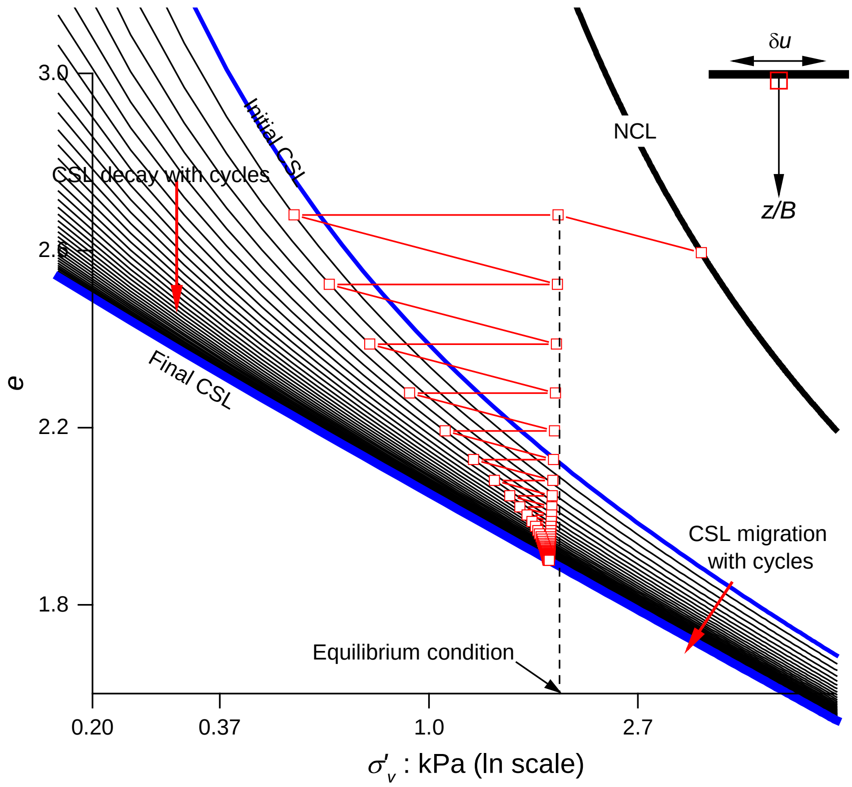

Figure 15. Vertical effective stress - void ratio space, showing state paths of a soil element at shearing interface, i.e. at $z = 0$.

12. LIST OF TABLES

Table 1. Framework parameters

Framework components	Parameter	Dimension	Description	Value	Notes on calibration or source of selected value
Boundary conditions	B	L	Foundation breadth	5 m	Test parameter
	L	L	Foundation length	10 m	Test parameter
	σ_{op}	m/LT^2	Operative vertical bearing pressure	1.85 kPa	Test parameter
Soil sample characteristics	γ_{av}'	m/T^{2}L^2	Unit weight of the soil (average)	5.9 kN/m^3	Obtained from moisture content data of soil core samples
	$[s_u/\sigma'_{v0}]_{\mathrm{NCL}}$	[-]	Normally consolidated strength ratio	0.15	Obtained from moisture content data of soil core samples, and in situ undrained shear strength of the soil sample as assessed from a T-bar penetrometer
	S_t	[-]	Soil sensitivity	2.4	Ratio of intact to fully remoulded shear strength obtained from cyclic T-bar penetrometer test
Void ratio - vertical effective stress relationship	N	[-]	Void ratio intercept at σ'_v = 1 kPa of the Normal Compression Line (NCL) in the $e - \ln\sigma'_v$ plane	2.447	Calibrated from moisture content data of soil core samples
	Δe_i	[-]	Additional void ratio at $\sigma'_v = \sigma'_{v,i}$, where virgin yielding begins	1.2	
	σ'_{vi}	m/LT^2	Initial vertical yield stress	1.5 kPa	
	b_{NCL}	[-]	Compression destructuring index, where $0 < b_{NCL} < \infty$	1	
	κ	[-]	Slope of swelling line	0.1	
	Γ_0	[-]	Void ratio intercept at σ'_v = 1 kPa of the initial Critical State Line (CSL) in the void ratio -natural logarithm of vertical effective stress ($e - \ln\sigma'_v$) plane	2.163	
	λ	[-]	Slope of NCL in the $e - \ln\sigma'_v$ plane	0.261	
Shear stress - vertical effective stress relationship	M	[-]	Slope of CSL in vertical effective stress - shear stress (σ'_v - τ) plane	0.92	Critical state parameter from Stewart (1992), Cocjin et al. (2014)
CSL migration/decay	R_0	[-]	Initial spacing ratio	7.978	Calibrated from moisture content data of soil core samples and in situ undrained shear strength of the soil sample as assessed from a T-bar penetrometer
	$N_{eq(95)}$	[-]	CSL migration parameter	40	Cycle number required for the current spacing ratio, R to be equivalent to 95% of the value of the final spacing ratio, R_f. Fitted based on model test observations.
	R_f	[-]	Final spacing ratio	19.148	Equivalent to the product of the initial spacing ratio and soil sensitivity, i.e.

					R_0S_t, calibrated as in R_0
Remoulding	β	[-]	Excess pore pressure parameter, represents the curvature of the σ'_v - τ effective stress path created by the generated excess pore pressure,	2	A parabolic curvature of the effective stress path in the stress plane was selected
	χ	[-]	Remoulding parameter, controls the fraction of the full pore pressure that is generated during shearing without failure	2.5	Selected to mimic a parabolic curvature of the effective stress path in the stress plane, and consistent with experimental observations
Consolidation parameters	T_{50}	[-]	Dimensionless time factor for 50 % of the consolidation settlement to occur	0.043	Obtained from a finite-element analysis of a rectangular sliding mudmat (see Feng & Gourvenec (2015))
	a	[-]	Void ratio - permeability relationship parameter	0.08	Obtained from Rowe cell tests on kaolin clay (see Sahdi 2014)
	α	[-]	Ratio of vertical to operative coefficient coefficient	2.7	Obtained from the dissipation response of a 'piezofoundation' reported in Cocjin *et al.* (2014)
	b	[-]	Void ratio - permeability relationship parameter	8.5	Obtained from Rowe cell tests on kaolin clay (see Sahdi 2014)
	m	[-]	Constant	1.05	Numerical solution for rectangular foundation taken from Feng & Gourvenec (2015)
Others	γ_w	m/T^2L^2	Unit weight of water	9.86	Universal constant

Table 2. Curve-fitting parameters for plastic strain ratio

Parameter	Value
Λ	0.008
v_0	0.27
ξ	0.5